Proceedings of ERAD (2004): 286–290 © Copernicus GmbH 2004

ERAD 2004

Cloud dynamical, microphysical and radiative properties retrieved from ground based radar/lidar synergy

D. Bouniol[1], A. Protat[1], J. Delanoë[1], and M. Haeffelin[2]

[1]Centre d'Etude des Environnements Terrestre et Planétaires, CNRS, Vélizy, France
[2]SIRTA, IPSL, Palaiseau, France

1 Introdiction

Representation of clouds in climate or forecast model is done (depending on the scale of the model) by using variables such as ice water content or effective radius. On the other hand dynamical variables (such as falling velocity) are used in order to get a realistic cloud life cycle. However due to a lack of observations these parameter can be over/under estimated by a factor of two.

In the framework of the CloudNET project vertically pointing Doppler cloud radar and lidar are continuously operated from three sites in Europe (SIRTA (France), Chilbolton (UK) and Cabauw (Netherlands)) and at the same time outputs of four operational models (ECMWF, UKMO, Météo-France and KNMI) are stored at the measurement points.

In order to derive microphysical and radiative parameters an adaptation of Tinel et al. (2004) radar/lidar algorithm has been performed. Algorithms making use of the radar Doppler signal to derive dynamical properties (Protat et al. (2002) and Bouniol et al. (2004)) have been developped and implemented. The retrieval of TKE disipation rate is here the subject of a companion paper and this method will not be described here. This paper will be focussed on the determination of other dynamical caracteristics and on the microphysical and radiative property retrieval.

As a first step the principle of radar/lidar synergetic algorithm is recalled, then it is explained how vertical air velocity and particles terminal fall speed are determined using the Doppler capability of the radar. These algorithms are applied to data collected on one site of the CloudNET project and some way for comparing these retrieval with models are suggested. Finally some conclusions and perspectives are given.

Correspondence to: D. Bouniol
(dominique.bouniol@cetp.ipsl.fr)

2 Principle of the retrieval of microphysical and radiative parameters

The principle of the radar/lidar algorithm is completely described in Tinel et al. (2004) for airborne instrument. It has been validated and compared to another algorithm making use of the same measurements Donnovan et al. (2000) in Hogan et al. (2004) for a space configuration. In order to derive microphysical and radiative parameters from continuously operated groud-based radar/lidar a new version of this algorithm has been developped.

This algorithm lies on the hypothesis that the radar reflectivity (Z) and lidar extinction (α) can be related to each other and then related to microphysical parameter such as ice water content (IWC) and radiative parameter, such as effective radius (r_e) using statistical relationships derived from in-situ measurements. However if one tries to derive a statistical relationship between for instance Z and IWC a large scatter is observed which makes hard a statistical relationship to be derived with accuracy. In order to reduce the scatter, it is rather looked for relationships between $Z/{N_0}^*$ and $IWC/{N_0}^*$ (see Delanoë et al. (2004) for details), where ${N_0}^*$ is a normalisation parameter of the drop size distribution (see Testud et al. (2001) for computation of this parameter) and in this case the particle size distribution can be rewritten as $N(D) = {N_0}^* F(D/D_m)$ where F is the shape function and D_m the median volumetric diameter.

The set of equations linking the measurements to the parameters to be retrieved and the measurements of the two instruments is called the inverse model and the one used is this paper is given in Eq. (1). This inverse model has been determined by Delanoë et al. (2004) on a large number of microphysical data sets and they show that it does not depend of the geographical location of the measurements and of the cloud type or altitude. However to derive these statistical relationships a density law needs to be assumed, in our case the law for spheric aggregates of Locatelly and Hobbs (1974) is used. The Rayleigh approximation being used in

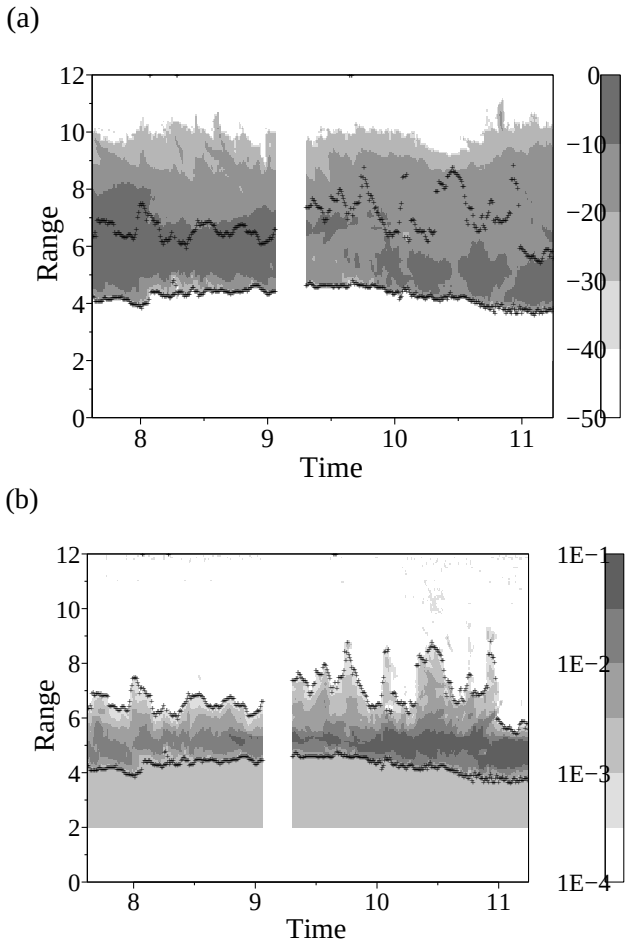

Fig. 1. Time series in [Hours] of (a) radar reflectivity in [dBZ] and (b) lidar backscatter coefficient in [$km^{-1}\,sr^{-1}$] as a function of range in [km] observed at SIRTA on the 14 April 2003. The crosses on both figures delimited the common sampling area of the two instruments.

order to compute the radar parameters.

$$\begin{aligned} \alpha &= s\ N_0{}^{*(1-t)}\ Z^t \ \text{ with s=5.5860 } 10^{-4} \text{ t=0.5875} \\ IWC &= p\ N_0{}^{*(1-q)}\ Z^q \ \text{ with p=8.6497 } 10^{-6} \text{ q=0.5638} \end{aligned} \quad (1)$$

where α is expressed in km^{-1}, $N_0{}^*$ is in m^{-4}, Z is expressed in $mm^6 m^{-3}$ and IWC in g m^{-3}.

In fact radar and lidar are not measuring Z and α respectively but the apparent reflectivity Z_a and the backscatter coefficient β_a (where we have $\alpha = k\beta$ with k the phase function), which correspond for both instruments to attenuated measurements. In order to simplify the problem, it is assumed that the radar signal is not attenuated within clouds, which can be translated as $Z = Z_a$. Figure 1 shows the time series of radar reflectivity (a) and lidar backscattering coefficient (b) observed at SIRTA (France) by the 94 GHz radar RASTA and the 532 nm lidar LNA on the 14 April 2003. It can be observed that both instruments detect the same cloud base (lower line of black crosses) that will be considered in the following as r_1 but not the same cloud top: the lidar do not penetrate the whole cloud depth. Then in the following the highest common observed altitude (highest line of black crosses on Fig. 1) will be considered as r_0.

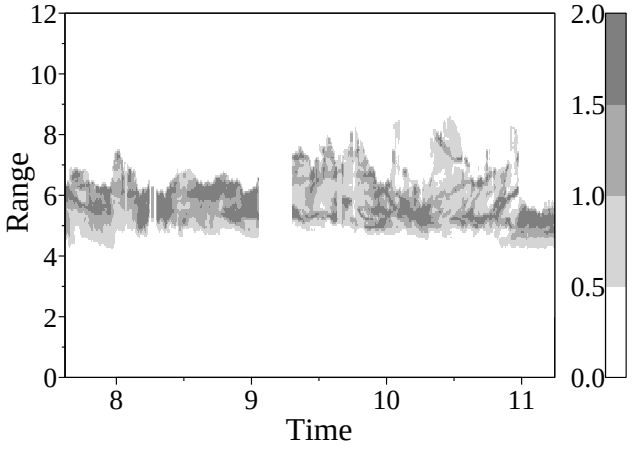

Fig. 2. Retrieved time serie in [hours] of α in [km^{-1}] from radar and lidar observations shown in Fig. 1 as a function of range in [km]

The first step of the processing consists in linking the two measurements. This is done by using an integral constraint, written as follows and assuming as a first step a constant profile of $N_0{}^*(r)$.

$$\int_{r_1}^{r_0} \alpha(z)dz = \int_{r_1}^{r_0} sN_0{}^*(z)^{(1-t)}Z(z)^t dz \quad (2)$$

where r_0 and r_1 are the upper and lower limits respectively of the common sampling area of radar and lidar (see Fig. 1) and s and t are the coefficients relating α and Z within the inverse model (Eq. 1). This equation can be rewritten as an $\alpha(r_0) = f(\alpha(r_0))$ equation and solved. Then the $\alpha(r_0)$ value found is introduced within the (Klett, 1981) solution rewritten as a function of extinction:

$$\alpha(r) = \frac{\alpha(r_0)\beta_a(r_0)}{\beta_a(r_0) + 2\alpha(r_0)\int_r^{r_0} \beta_a(z)dz} \quad (3)$$

This leads to a new profile of $\alpha(r)$ and then by using the α/Z law of the inverse model (1) to a new profile of $N_0{}^*(r)$ which is re-introduced within Eq. (2). This process is carried on up to the convergence to a $N_0{}^*(r)$ profile. Once this profile is obtained it is introduced within the inverse model and then IWC profile is computed. r_e profile is deduced from IWC and α profile using:

$$r_e = \frac{3}{2\rho_i}\frac{IWC}{\alpha} \quad (4)$$

with ρ_i the density of pure ice.

Figure 2 shows the lidar extinction obtained using this iterative process. It has to be mentionned that since this parameter is computed using Eq. (3) it has poor sensitivity to the density law introduced to derive the inverse model

(Eq. 1). Indeed test has been performed on simulated profiles by using different inverse models computed with different density laws and the resulting error on retrieved profile remains nearly constant. This means that for instance the optical depth which can be computed from this parameter is not sensitive the density law introduced in the inverse model.

The microphysical (IWC and $N_0{}^*$) parameters and radiative parameter (r_e) are shown on Fig. 3a and b and c respectively. It can be observed that even the retrieval algorithm is performed radial by radial, horizontal consistency is observed. IWC field (Fig. 3a) shows the expected behaviour with a decrease of its values at cloud base due to evaporation of ice particles. The $N_0{}^*$ parameter can be used to retrieve drop size distribution everywhere within the cloud. Indeed it has been demonstrate (Delanoë et al., 2004) that the shape function (F) is fairly stable. Then by knowing $N_0{}^*$ and deducing D_m from the retrieved parameters one can re-compute the drop size distribution at each point of the retrieval. r_e seems to give values in good order of magnitude (may be a bit small) with what is expected in such clouds.

3 Principle of the retrieval of dynamical parameters

By using the high temporal resolution of mean Doppler velocity ($\overline{v}$) measurements by vertically pointing cloud radar, TKE dissipation rate can be computed (Bouniol et al., 2004). Another use of this measurement can be performed in order to separate the contribution of the air vertical velocity w and the terminal fall speed of hydrometeors V_t. The method sumerised, in (Protat et al., 2002) or (Orr and Kroppfli , 1999), consists in deriving statistical $V_t = aZ^b$ relationships. Indeed, within weakly-precipitating clouds, the vertical air motions are generally small. In any case, however, the vertical air motions not negligible with respect to terminal fall speed. For a long time span, however (a few hours), the mean vertical air motions should vanish with respect to the mean terminal fall speed. This method can only be used if no radar attenuation is present, which is the case within clouds when no low water clouds are present.

Figure 4 illustrates the observed mean Doppler velocity for the same day as previously. The following method is then applied to the data shown on Fig. 1a and 4.

As a first step, the a and b coefficients are determined by fitting in the least squares sense the observed $(Z, \overline{v})$ couples. Once the coefficients are obtained the V_t/Z relationship is applied to the reflectivity leading to the V_t field. Then, by substracting this V_t to $\overline{v}$ one can obtain the w field.

Figure 5a and b show V_t and w fields respectively derived from the radar measurements of the 14 April 2003 using the method of Protat et al. (2002). As expected the largest value of terminal speed are ecountered in the lower levels of the clouds, as w do show evidence of particular feature.

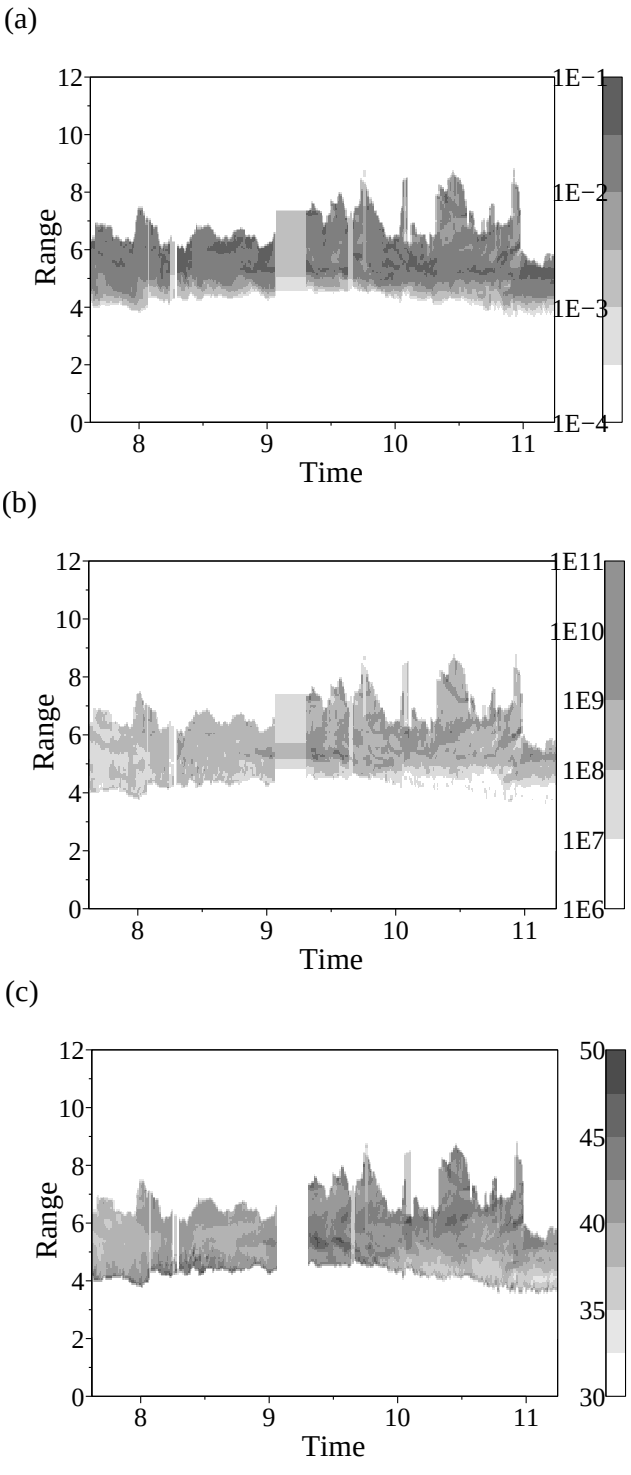

Fig. 3. Retrieved time series in [Hours] of (a) IWC [g m^{-3}], (b) $N_0{}^*$ [m^{-4}] and (c) r_e in [μm] from radar and lidar observations shown in Fig. 1 as a function of range in [km].

4 Products for model comparisons

The previous section has shown how an observed cloud can be characterised on microphysical, radiative and dynamical

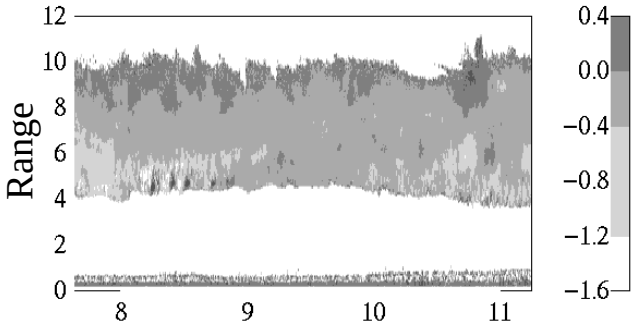

Fig. 4. Measured time series in [Hours] of mean Doppler Velocity [m s^{-1}] as a function of range in [km].

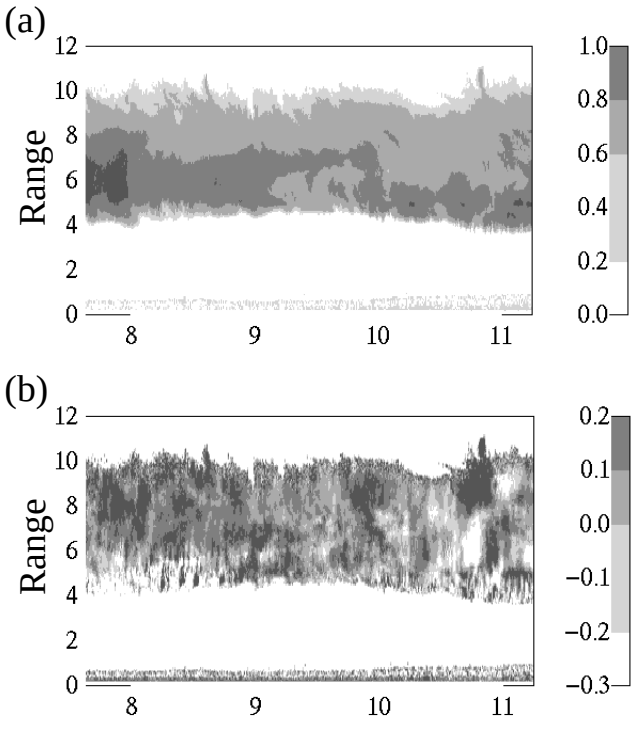

Fig. 5. Retrieved time series in [Hours] of (a) V_t in [m s^{-1}] and (b) w in [m s^{-1}] as a function of range in [km].

point of view. Tha aim of the CloudNET project is to compare observation derived and model derived physical parameters. In order to make easier these comparisons one needs to determine the behaviour of such parameters on a statistical point of view.

Figure 6 show histograms of IWC (Fig. 6a) and r_e (Fig. 6b) of the retrieved values for the 14 April 2004. The more frequent values of IWC are encountered in the classe 110^{-2} to 110^{-1}. It appears on this figure that the histograms of IWC is not symmetric showing more low values than high and that its range of variation is larger than the one of r_e. Indeed r_e histogram (Fig. 6b is peaking strongly for values between 37.5 μm and 42.5 μm. These histograms are made at the scale of the retrieval, however if one want to compare with models they need to be degraded at the model resolution

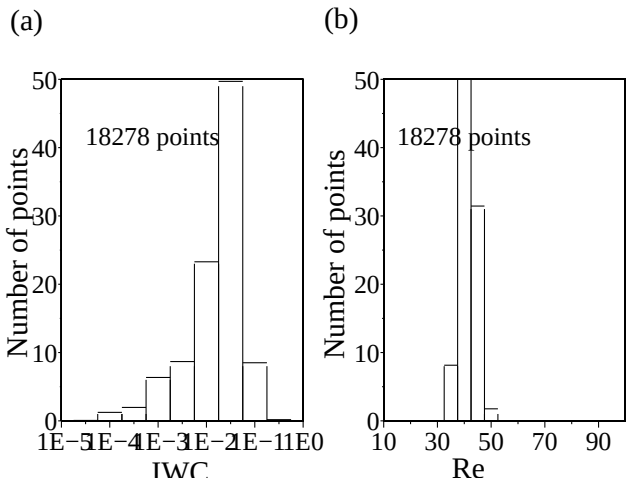

Fig. 6. Histograms of retrieved (a) IWC [g m^{-3}] (b) r_e [μm]

(in our case UKMO, RACMO, ARPEGE and ECMWF). The results are not shown here, but generally the models show a range of variation as large as their resolution is small and are generally peaking on a given class.

Another way to compare observations and models is to directly compare parametrization or relationships between two physical parameters. Two such relations are shown on Fig. 7a and b. These two plots show a large scatter, however superimposed to the general tendancy it seems to exist different regions within the scatter plot which suggests that it is necessary to introduce a third parameter within the scatter which could be for instance altitude or cristal shape. For example it seems to exist a linear (in log scale for IWC) relationships between IWC and V_t (Fig. 7a. When IWC increases, V_t increases. This result is not surprising, it means that when a particles is denser it falls faster. However one can distinguish an enlargement of the scatter for large IWC. The second scatter plot (Fig. 7b) showing r_e as a function of V_t is a bit suprising, indeed it shows that V_t is increasing when r_e is decreasing. This would mean that small particles are denser than the largest and then will fall comparatively faster. However even if a particle is less dense, the fact to be larger should make it heavier and then falling faster. At this point further investigations are needed, in particular concerning the density law introduced in the inverse model.

5 Conclusion

Several algorithm are routinely applied to continuously operating ground-based radar and lidar measurements at three sites in Europ. Microphysical and radiative parameters are derived using a synergetic algorithm, terminal fall speed and air vertical velocity are derived using a statistical approach and TKE energy is deduced by using the high temporal resolution of radar measurements. These algorithms were described and illustrated by their applications to an ice cloud observed on the 14 April 2003. At this point some

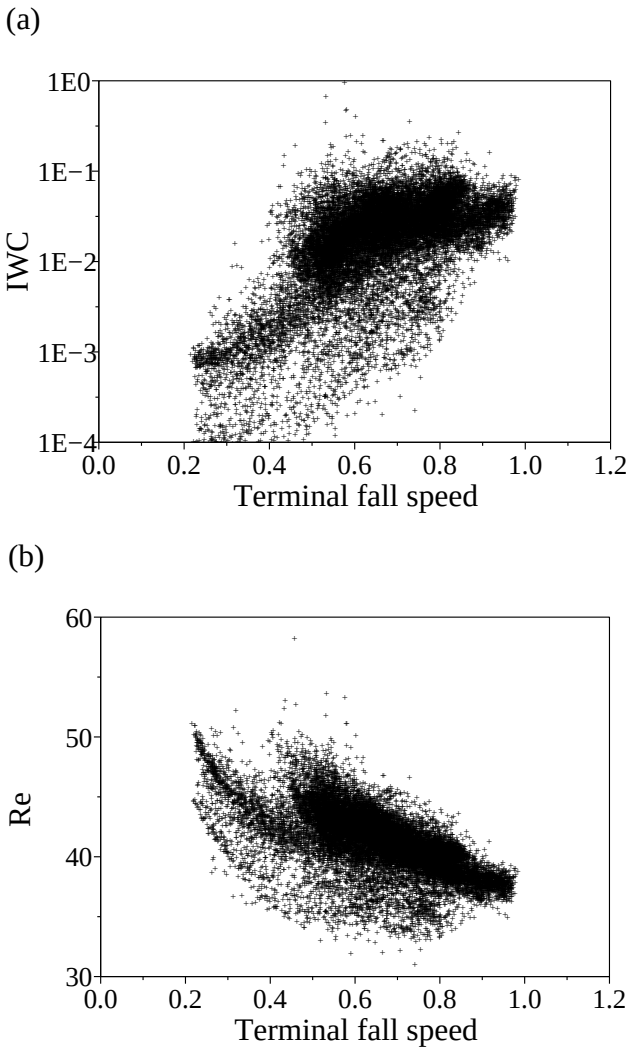

Fig. 7. Scatter plots of (a) IWC in [g m^{-3}] as a function of V_t in [m s^{-1}] and (b) r_e in μm as a function of V_t [m s^{-1}.]

improvement seems necessary in this algorithm. As shown a density law (Locatelly and Hobbs (1974) for spheric aggregates in the present case) needs to be introduced in order to build the inverse model, it can be imagined to build several inverse model with different density law in order to used to adapt the inverse model to the type of clouds. Mie effects need also to be introcuded within the synergetic algorithm. It has been observed that the common area between radar and lidar is about half of the clouds. If one want to compare more extensively observation derived microphysical and radiative parameters with models it would be interesting to complete this retrieval with a radar only and lidar only method which used the results of the synergetic algorithm and allow to derive the parameters when only one instrumennt is present.

Finally, different ways to compare observations with models were suggested. Such comparisons extended to other cases and other sites will be shown during the presentation.

The same case study is under simulation using a mesoscale model including a specific parametrisation for ice clouds. The output obtained from observations will then be compared with the same paremeters obtained from the model. As a second step of simulation, the statistical relationship derived from observations will be introduced in the model, to study their influence on the simulated cloud life cycle.

Acknowledgements. The RASTA 94 GHz radar was developped with support from Centre National d'Etudes Spatiales and Institut des Sciences de l'Univers. We are all indebted to the technical staffs that helped to develop the radars and conduct the CloudNET operations.
This research received funding from the European Union CloudNET project (grant EVK2-CT-2000-00065).

References

Bouniol, D., Hogan, R. J., Illingworth, A. J., and Protat, A.: Eddy dissipation rate from 94 GHz Doppler radar, to be submitted to J. Atmos. Oceanic Technol., 2004.

Delanoë, J., Protat, A., Testud, J., and Bouniol, D.: Statistical properties of normalized ice particle distributios from in-situ microphysical measurements. Part II: Establishment of an "universal" statistical model for radar-lidar inversion techniques, to be submitted to J. Appl. Meteor., 2004.

Donnovan, D. P., van Lammeren, A. C. A. P., Russchenberg, H. W. J., and Apituley, A.: Cloud effective particle size and water content profile retrievals using combined lidar and radar observations, Part I: theory and simulations, J. Geophys. Res., 106, 27 425–27 448, 2000.

Hogan, R. J., Donovan, D. P., Tinel, C., Brooks, M. A., Illingworth, A. J., and Poiares Baptista, J. P. V.: Independent evaluation of the ability of spaceborne radar and lidar to retrieve the microphysical and radiative properties of ice clouds, to be submitted, 2004.

Klett, J. D.: Stable Analytical Inversion for processing lidar returns. Applied Optics, 20, 2, 211–220, 1981.

Locatelly, J. and Hobbs, P.: Fall speeds and masses of solid precipitation particles, J. Geophys. Res., 79, 2185–2197, 1974.

Orr D. W. and Kroppfli, R. A.: A method for Estimating Particle Fall Velocities from Vertically Pointing Doppler Radar, J. Atmos. Sci., 29–37, 1999.

Protat, A., Tinel, C., and Testud, J.: Dynamic properties of water and ice clouds from dual beam cloud airborne radar data: the CARL2000 and CARL2001 validation campaign, 11th Conference on Cloud Physics, 3–7 June 2002, Ogden, UT, USA, 2002.

Testud, J., Oury, S., Black, R. A., Amayenc, P., and Dou, X. K.: The concept of "normalized" distribution to describe raindrop spectra: a tool for cloud physics and cloud remote sensing, J. Appl. Meteor., 40, 1118–1140, 2001.

Tinel, C., Testud, J., Pelon, J., Hogan, R., Protat, A., Delanoë, J., and Bouniol, D.: The retrieval of ice cloud properties from cloud radar and lidar Synergy, in revision J. Appl. Meteor, March 2004.